EFDA–JET–PR(09)15

A. Murari, J. Vega, D. Mazon, G.A. Rattà, J. Svensson, G. Vagliasindi, D. Alves, P. Arena, C. Boulbe, R. Coelho, B. Faugeras, L. Fortuna, D. Moreau, D. Testa and JET EFDA contributors

Innovative Signal Processing and Data Analysis Methods for Control in Reactor Relevant Devices

Innovative Signal Processing and Data Analysis Methods for Control in Reactor Relevant Devices

A.Murari[1], J.Vega[2], D.Mazon[3], G. A. Rattà[2], J.Svensson[4], G.Vagliasindi[5], D.Alves[6], P. Arena[5], C. Boulbe[7], R.Coelho[6], B. Faugeras[7], L.Fortuna[5], D. Moreau[3], D.Testa[8] and JET EFDA contributors*

JET-EFDA, Culham Science Centre, OX14 3DB, Abingdon, UK

[1]Consorzio RFX-Associazione EURATOM ENEA per la Fusione, I-35127 Padova, Italy.
[2]Asociación EURATOM-CIEMAT para Fusión, CIEMAT, Madrid, Spain Association
[3]EURATOM-CEA, CEA Cadarache, 13108 Saint-Paul-lez-Durance, France
[4]Max-Planck-Institut für Plasmaphysik, Teilinstitut Greifswald, EURATOM Association, Wendelsteinstr.1,17491 Greifswald, Germany
[5]Dipartimento di Ingegneria Elettrica Elettronica e dei Sistemi-Università degli Studi di Catania, 95125 Catania, Italy
[6]EURATOM-IST Association, IPFN, IST, 1049-001 Lisboa, Portugal
[7]Laboratoire J-A Dieudonné (UMR 66 21), Université de Nice Sophia-Antipolis, CNRS Parc Valrose 06108 Nice Cedex 02 France
[7]Centre de Recherches en Physique des Plasmas,Association EURATOM - Confédération Suisse École Polytechnique Fédérale, CH-1015 Lausanne, Switzerland
** See annex of F. Romanelli et al, "Overview of JET Results", (Proc. 22 [nd] IAEA Fusion Energy Conference, Geneva, Switzerland (2008)).*

Preprint of Paper to be submitted for publication in
Nuclear Fusion

ABSTRACT.
The steady state burn of fusion plasmas will require a significant increase in the amount and sophistication of feedback control with respect to present day experiments. In the last years, it has been realised that more involved real time schemes need significant advances in the signal processing and data analysis methods. Since one of the crucial issues for the control of reactor relevant configurations is the proper identification of the plasma to be controlled, various methods for the determination of the magnetic topology are being developed at JET. In addition to a real time algorithm (EQUINOX) to solve the Grad-Shafranov equation on a time scale of ms, a new approach based on Bayesian statistics is also providing very reliable and fast results. Robust methods of confinement regime identification are a prerequisite for safe, general control schemes. New identifiers based on Support Vector Machines have been developed and they have success rates exceeding 99% in determining whether plasmas are in the L or H mode. Prediction of harmful events is also an important issue in the perspective of safely operating reactor relevant devices. A new disruption predictor based on Support Vector Machines is being developed and has already provided success rates higher than 90% in realistic real time conditions. Moreover, the generalisation capability of this new predictor has been confirmed by applying it to new experimental campaigns not used for the training. The success rate remains high even more than ten campaigns, which means more than three years, after the last one used for the training. The enormous progress of video camera technologies in the last decades has increased the range of applications of image diagnostics. Their deployment in real time requires the development of new image processing algorithms. The innovative technology of Cellular Nonlinear Networks has already been implemented successfully on JET for the real time identification of hot spots. A series of new feedback schemes has also been explicitly developed not much to control the plasma but to really improve the physics understanding of some phenomena. Particularly interesting are the simultaneous control of the safety factor and pressure profiles and the real time tracking of Toroidal Alfven Eigenmode instabilities. These advanced feedback schemes for physics understanding often require more advanced signal processing techniques like adaptive filtering.

1. INTRODUCTION

Even if the long term goal of Magnetic Confinement Nuclear Fusion (MCNF) is the sustained, steady state burn of high temperature plasmas, nowadays even in the most sophisticated devices many parameters are still set in advance and not controlled in feedback during the discharges. A typical example is the confinement regime, and in particular the H mode, and the Advanced Scenarios (AS) with Internal Transport Barriers (ITBs). The plasma is assumed to access the H mode or trigger an ITB when the power input reaches a certain threshold and the times for the onset of these two types of regimes are fixed in advance and not detected in real time. In case of anomalous behaviour of the discharge, for whatever reason, if the plasma is not in the expected confinement regime, the feed forward control can be inadequate; the other active feedback controls can have a

detrimental effect on the performance and even increase the chances of disruptions. Another important aspect of the plasma configuration, which is not sufficiently controlled in feedback, is certainly the internal topology of the magnetic fields. Even if the plasma boundary is typically well determined and controlled in practically all present day devices, the internal current profile is not.

One of the main difficulties, which has prevented so far a more systematic use of real time feedback in MCNF, is certainly the problem of the identification of the plasma. i.e. the proper measurement of the plasma parameters relevant to the control objectives. Any form of control requires a careful determination of the system status and this is a major challenge in the case of thermonuclear experiments. Even if in modern machines the parameters of the discharge are measured by a wide range of diagnostics, deriving sound and reliable information in the short time available for control has proved to be a significant difficulty in the last decades. One of the reasons, for the relative slow pace of progress in this field, has certainly been the lack of data analysis tools adequate for control. Indeed the offline analysis methods developed to understand the physics behaviour of the plasma do not have the same objectives as the real time feedback and therefore are not always satisfactory in this respect. In modern, reactor grade Tokamak machines the data processing for control is complicated by several issues. First of all many quantities have to be measured. Secondly the amount of information to be processed can be enormous. JET real time system includes about 30 diagnostics for a total number of more than 50 signals to be handled by the Asynchronous Transfer Mode (ATM) network. Another important peculiar aspect of control for Fusion to be kept in mind is the fact that high temperature plasmas are systems very difficult to access for measurement. A lot of crucial information is therefore derived from measurements taken outside the plasma exploiting their natural emission. The interpretation of these signals needs solving sophisticated inversion problems, which are difficult, sometimes ill-posed and can require significant computational resources. This is aggravated by the nonlinear interactions between various phenomena and subsystems.

In this paper various innovative data analysis tools, explicitly conceived for application of feedback control in a Tokamak environment, are reviewed. They have been tested on JET and therefore they are expected to provide a good reference for the development of analogous techniques in ITER. First of all, to address the real time determination of the magnetic topology, a couple of alternative methodologies are described: the first is based on a fully probabilistic treatment based on Bayesian statistics [1], the second on a more traditional solution of the Grad-Shafranov equation [2] (see section 2.1). A very powerful hybrid method, combining Support Vector Machines (SVMs) with the Parzen window using Bayes formula [3], is shown to be able to identify whether the plasma is in the H or L mode of confinement with practically 100% success rate within the error bars of the measurements (see section 2.2). Some advanced data analysis techniques have also been applied to the issue of prediction. In Tokamak operation, the main event to avoid is certainly disruptions, which are not only harmful to the experimental programme but can also severely damage the device. Some refinements of the SVM methodology have been explicitly implemented for this purpose and

have allowed an unprecedented level of accuracy on a large JET database of disruptive discharges (see section 3). The developed controllers are very robust and their prediction capability remains very high even more than ten campaigns, covering and interval of more than three years, after the last one used for the training; it is worth mentioning that this capability has been verified using a database of more than 2000 discharges, the largest one even considered to test machine learning applications for disruption prediction. In the last years, the improvements in camera technologies have allowed a much higher deployments of video diagnostics in fusion. On JET the number of instruments using cameras, both visible and infrared, has increased significantly and now some of them can produce even Gbytes of data per shot. New methods and techniques to make use of all this information for feedback purposes are therefore strongly required. The technology of Cellular Nonlinear Networks [4] has been successfully deployed to analyse in real time infrared images and detect hot spots on JET inner wall (see section 4). The use of feedback control for direct study and understanding of physical phenomena has become much more common recently with the installation of two new sets of antennas [5] to excite and study Toroidal Alfven Eigenmodes (TAE) [6] (see section 5). Real time tracking of TAE modes provides a lot of information about the properties of these instabilities, like their damping rate. Another important subject is the simultaneous control of both the current and pressure profiles. In addition to the operational relevance, these studies are expected to help clarify the physics of ITB triggering [7]. Feedback for physical understanding requires often more sophisticated real time signal processing than usually available and indeed in the last years a lot of progress has been made in adaptive filtering techniques like the Kalman filter [8] for various applications (see section 6). The new prospects of advanced signal processing and data analysis tools for feedback control are reviewed in the last section of the paper.

2. IDENTIFICATION: MAGNETIC TOPOLOGY AND CONFINEMENT REGIME

2.1 MAGNETIC TOPOLOGY

An important weakness of practically all present day feedback schemes for Tokamak plasmas is the lack of a reliable real time identification of the magnetic topology. The plasma boundary is routinely determined and controlled in many devices but when it comes to the internal configuration of the fields, only offline codes are available. They are typically based on the solution of the Grad-Shafranov equation, which assumes complete equilibrium between the magnetic and kinetic pressure inside the plasma. In the main implementations of the Grad-Shafranov equation in the codes for the determination of the magnetic topology, like EFIT [9], additional hypotheses about the physics are normally assumed, like zero plasma velocity or the absence of plasma currents at the separatrix. In order to avoid assumptions about the physics and to provide directly an interval of confidence on the magnetic reconstructions, a different method, purely probabilistic and based on Bayesian statistics, is being tested in JET [10]. In this approach, the plasma and the surrounding structures are modelled with a series of current beams. The configuration of the internal fields is determined by calculating the most probable distribution of the currents in the beams given the measurements available. The

full implementation of this method requires the complete statistical model of the diagnostics providing the measurements used to reconstruct the fields. Properly devising such models can be a quite labour intensive task but the advantages are potentially very significant. First of all a coherent and complete estimate of the confidence intervals can be provided directly since the approach is probabilistic in nature. Secondly no assumptions about the physical behaviour of the system are made and therefore the exploitation of the available information in the measurements is maximised.

An example of the results is shown in figure 1, where the obtained magnetic topology for both limiter and X point configurations are reported, together with the confidence intervals in the most important topological parameters of the magnetic configuration.

Since significant efforts have been devoted to obtain an analytical solution for the inversion problem, no iterations are required and therefore the approach can also be easily used for feedback control. Even without any particular optimisation to improve real time performance, the computational time required is already more than acceptable. As an example, in figure 2 it is shown how the magnetic topology with the highest posterior probability for a JET discharge is calculated in about 1 ms on a 2GHz clock laptop computer. The good performance in terms of speed is good enough to provide even the confidence interval in real time. An example of this is also shown in figure 2. The formulation of the uncertainty intervals is a bit more computation intensive but, with a minimum of optimisation, this can also be easily provided with a time resolution of the order of tens of ms and therefore still within the constraints of typical real time applications. Another important advantage of the Bayesian method is that any constraint or smoothing can be accommodated in the "a priori" probability of the Bayesian treatment. For feedback control several alternatives are potentially promising. Priors derived from similar previous discharges are expected to be often adequate but also additional information obtained from other sources, like simulations or theoretical models can also be accommodated. Moreover the method is perfectly suited to exploit the synergy between different measurements techniques. The information of diagnostics different from the traditional pickup coils can be integrated inside a unique estimator. In particular, the positive impact of internal measurements of the magnetic fields is illustrated in figure 3, which shows the improvement in the uncertainty intervals which can be achieved by combining the measurements of different systems.

Despite the fact that the method just described is quite fast to compute and potentially very innovative, it is necessary to compare its results with some more traditional methods, which solve the Grad Shafranov equation

$$-\nabla^{*}\psi = rp'(\psi) + \frac{1}{\mu_0 r}(ff')(\psi) \tag{1}$$

with $\psi(r,z)$ the poloidal flux and ∇^{*} the linear elliptic operator, defined as

$$\nabla^{*} = \frac{\partial}{\partial r}\left(\frac{1}{\mu r}\frac{\partial}{\partial r}\right) + \frac{\partial}{\partial z}\left(\frac{1}{\mu r}\frac{\partial}{\partial z}\right) \tag{2}$$

in which μ_0 is the magnetic permeability of vacuum.

The magnetic field can be decomposed as $B=B_p+B_\phi$ where $B_p=(Br, Bz)$ is the poloidal component and B_ϕ is the toroidal component. Using this decomposition, the poloidal flux $\psi(r,z)$ can be expressed as follows:

$$\begin{cases} B_r = -\dfrac{1}{r}\dfrac{\partial \psi}{\partial z} \\ B_z = \dfrac{1}{r}\dfrac{\partial \psi}{\partial r} \end{cases} \tag{3}$$

If e_f indicates the unit vector in the toroidal direction and ψ the diamagnetic function, the poloidal and toroidal component of the magnetic field can been written as in the following formulas:

$$\begin{cases} B_p = \dfrac{1}{r}\left[\nabla \psi \; x \; e_\phi\right] \\ B_\phi = \dfrac{f}{r} e_\phi \end{cases} \tag{4}$$

The right hand side the Grad Shafranov equation involves the functions $p(\psi)$ and $f(\psi)$, which are not directly measured inside the plasma. It can also be noted that in vacuum, where no plasma currents are present, the magnetic flux y satisfies:

$$\nabla^* \psi = 0 \tag{5}$$

In order to find the plasma equilibrium, the non linear bidimensional differential Grad Shafranov equation (1) must be solved. The right hand side of this equation is composed of two functions representing the pressure p and the diamagnetic function f. The numerical identification problem is formulated as a least-square minimization based on available measurements with a Tikhonov regularization [11]. In the present version of the solver, the experimental measurements that are planned to be used for the identification are the magnetic pick-up coils on the vacuum vessel, the interferometric and polarimetric measurements and the Motional Stark Effect (MSE). From the flux loops measurements located around the vacuum vessel, the poloidal flux $\Psi(M_i)=h_i$ on particular positions M_i on Γ can be derived,

$$\psi(M_i) = h_i \quad on \quad \Gamma \tag{6}$$

where Γ is the reference surface outside the plasma.

Thanks to an interpolation between the points M_i, these measurements provide the Dirichlet boundary conditions h_i. The magnetic probes give the component of the magnetic poloidal field which is tangent to the vacuum vessel:

$$-\frac{1}{r}\frac{\partial \psi}{\partial n}(N_i) = g_i \tag{7}$$

The interferometric measurements provide the density integrals over the chords C_i

$$\int_{C_i} n_e(\overline{\psi})dl = \beta_i \tag{8}$$

where n_e represents the electronic density which is approximately constant on each flux surface. The polarimetric measurements give the Faraday rotation of the polarization angle of infrared laser radiation crossing the plasma along the same chords C_i as the interferometer:

$$\int_{C_i} n_e(\overline{\psi})B_{//}dl = \int_{C_i} \frac{n_e(\overline{\psi})}{r}\frac{\partial \psi}{\partial n}dl = \alpha_i \tag{9}$$

In the last relation the component of the poloidal field tangent to C_i is $B_{//}$ and d/dn represents the normal derivative of Ψ with respect to C_i.

The Motional Stark effect (MSE) angle gi is taken at different points $x_i=(r_i,zi)$:

$$tan(\gamma_i) = \frac{a_1 B_r + a_2 B_z + a_3 B_\phi}{a_4 B_r + a_5 B_z + a_6 B_\phi} \tag{10}$$

and can be linked to the local pinch of the magnetic field lines.
The problem is thus reduced to finding a solution that minimizes a cost function defined as:

$$J(A, B, n_e) = J_0 + K_1 J_1 + K_2 J_2 + K_3 J_3 + J_\varepsilon \tag{11}$$

with

$$\begin{aligned} J_0 &= \sum_i \left(\frac{1}{r}\frac{\partial \psi}{\partial n}(N_i) - g_i \right)^2 \\ J_1 &= \sum_i \left(\int_{C_i} \frac{n_e}{r}\frac{\partial \psi}{\partial n}dl - \alpha_i \right)^2 \\ J_2 &= \sum_i \left(\int_{C_i} n_e dl - \beta_i \right)^2 \\ J_2 &= \sum_i (mse - \gamma_i)^2 \end{aligned} \tag{12}$$

with mse the reconstructed measurement and K1 to K3 the weighting parameters enabling to give more or less importance to the corresponding experimental measurements. The inverse problem of the determination of A and B is ill posed. Hence a regularization term has to be used to converge on stable solutions. The Tikhonov regularization term J_e constrains the function A, B and n_e to be smooth enough and reads:

$$J_{\varepsilon} = \varepsilon_1 \int_0^1 [A''(x)]^2 dx + \varepsilon_2 \int_0^1 [B''(x)]^2 dx + \varepsilon_3 \int_0^1 [n_e''(x)]^2 dx \tag{13}$$

where ε_1, ε_2 and ε_3 are the regularizing parameters.

Recently at JET an ambitious project has been launched to implement and validate accurately the method previously described with a new specific code called EQUINOX [11] explicitly developed for real-time applications. The version of the code using only magnetic measurements has already been completely validated. A set of 130 JET discharges has been carefully selected exactly for this purpose. This database covers the vast majority of JET operational space. The plasma current range covered is between 1.12 and 3.09 MA, the magnetic field is between 1.68 and 3.42 T, the range in triangularity is $0.06<\delta<0.51$. It is also worth mentioning that also advanced scenarios like the hybrid have been included. The validation strategy consists of comparison of the EQUINOX results of global and local quantities with EFIT, the reference code at JET for magnetic reconstructions. Some of the most important plasma parameters which have been compared systematically are: the plasma volume, the plasma current, the safety factor at 95% of the minor radius, the safety factor on axis, the plasma internal inductance, the poloidal beta, the horizontal and vertical position of the X point. For the main parameters of the last closed flux surface, the EQUINOX estimates have also been compared with the code used at JET for boundary control: XLOC. All these tests have given very positive results. In figure 4 the time evolution of the radial position of the $\beta_{pol} + l_i/2$ is reported, together with a statistical comparison of the distance RIG between the last closed magnetic surface and the inner wall in the equatorial plane. It is worth mentioning that an evaluation of the sensitivity of the code to the magnetic measurement errors is also being performed. The validation of the version of EQUINOX including internal magnetic measurements (polarimetry and MSE) is under way together with the cross validation with the Bayesian approach.

2.2 CONFINEMENT REGIME IDENTIFICATION

In the ASDEX device it was discovered in 1982 that, increasing sufficiently the input power, the plasma tended to transit spontaneously to an enhanced confinement mode called the High confinement or H-mode [12]. The H-mode is characterized by the presence of a thin, edge region of very low transport. Steep gradients in the density and temperature profiles are observed across this layer, which is commonly referred to as the 'H-mode pedestal'. The thickness of the pedestal is typically 1-5% of the radius of the plasma, and therefore on JET the measured pedestal widths are of the order of a few centimetres. The low transport region at the edge of the H-mode plasma is known as the Edge Transport Barrier (ETB). Once the correct conditions are met, the transition from L to H mode occurs with the spontaneous formation of an ETB and, once the ETB is starting to develop, the confinement at the edge of the plasma improves with consequent further growth of the H-mode pedestal.

The first step, in the work described in this section, is the off-line training of a classifier for the

application to the real time identification of the confinement regime, L or H mode, in JET. The approach adopted has been a "hybrid classifier" [3], combining via the Bayes formula a SVM system with a non parametric statistical classifier based on the Parzen window.

SVM is a universal constructive learning procedure, based on statistical learning theory [13]. It consists of projecting the feature vectors into a high dimensional space – typically of much higher dimensions than the original feature space. With an appropriate linear or nonlinear mapping to a sufficiently high dimensional space, data from two categories can always be separated by a hyperplane. In more detail, given a training set of ℓ samples $(\mathbf{x}_1, y_1),...,(\mathbf{x}_\ell, y_\ell)$ $x_i \in \Re^n$ in the case of a binary classification problem (*i.e.* $y_i \in \{+1, -1\}$), SVM proceeds estimating the following decision function:

$$D(\mathrm{x}) = \sum_{i=1}^{l} \alpha_i \, y_i H(x_i, x) \tag{14}$$

$H(\mathbf{x}_i, \mathbf{x})$ is a kernel function [14] and the parameters α_i, i = 1,...,ℓ are the solutions of the following quadratic optimization with linear constraints:
maximization of the functional

$$Q(\alpha) = \sum_{i=1,1}^{ll} \alpha_i - \frac{1}{2} \sum_{i=j,1} \alpha_i \alpha_j y_i \, y_j H(x_i, x) \tag{15}$$

subject to the constraints

$$\sum_{i=1}^{l} y_i \alpha_i = 0, \quad 0 \le \alpha_i, \le \frac{C}{l} \; i = 1,...,l \tag{16}$$

where C is a regularization parameter.
The data points $\mathbf{x}_i$ associated with the nonzero α_i are called support vectors. Once the support vectors have been determined, the SVM decision function can be expressed as

$$\mathrm{D(x)} = \sum_{\text{support vectors}} \alpha_i y_i H(\boldsymbol{x}_i, \boldsymbol{x})$$

where $D(\mathbf{x})$ is the distance of the feature point to the hyper-plane that separates the two classes and, hence, the hyper-plane points satisfy $D(\mathbf{x}) = 0$.

The rule to classify a feature vector as L mode (class C_L) or H mode (class C_H) can be expressed as:

if sgn (D(**u**)) ≥ 0
u ∈ C_L
otherwise
u ∈ C_H
where sgn(t) is the sign function.

The database, used to assess the performance of the predictor developed for JET, is a set of 50 discharges, with the divertor MARKII Gas Box with the Septum, for which the transition times have been determined by the experts with a high degree of confidence [15]. Only for 42 shots all signals are available during 2s segments around the transition from low (L) to high (H) confinement regime. 80% of them are used for training purposes (33) and the rest constitute the corresponding test set. Regarding the H/L transition, 48 shots have been analysed by the specialists. Only 38 discharges have all the signals available during 2 s around the transition and again, an 80% of them (30 shots) are used for the training and the remaining ones for the test.

To study JET L/H transitions, 35 signals have been selected, on the basis of expert knowledge, to provide the basic information to discriminate between the L and H mode phases of the discharges. They include also geometrical parameters to take into account the position/shape of the plasma inside the vacuum vessel. The signals have then been provided as inputs to a tree structured methodology for classification: CART (Classification And Regression Trees) [16]. The CART outputs provide as result the variable ranking of the most relevant signals for the classification problem. For JET discharges with the Septum divertor configuration, six signals are determined as the most important ones for the L/H transition (table I) and a different set of six variables for the H/L transition [17].

Therefore, the feature vectors to identify the confinement regime belong to a 6-dimensional space, where each coordinate is the value of one of the physical quantities that appear in table I. It should be emphasised that these quantities correspond to the same time instant. They have also been properly normalised according to the relation

$$\frac{M - min(M)}{max\ (M) - min(M)} \tag{17}$$

so that they all assume values in the interval [0,1], in order to avoid bias in the classification due to the different numerical amplitudes of the various quantities.

Instead of using SVM, the classification problem can be addressed with more classical statistical methods and in particular density estimators. Probability density estimators are mathematical expressions which can be used to derive a probability distribution function from individual samples. Among the various non-parametric probability density estimators, the Parzen window method is one of the most widely used [18]. For univariate distributions, i.e. probability distributions depending on just one variable, the kernel estimator is given by

$$p(x) = \frac{1}{l\,h} \sum_{i=1}^{l} K\left(\frac{x - X_i}{h}\right) \tag{18}$$

where ℓ is the number of samples, h the window width and the function $K(t)$ is called a kernel. The above equation expresses the estimate of as an average of functions of x and the samples X_i. Practically, $K(t)$ is used for interpolation and each sample contributes to the estimate depending on its distance from x. $K(t)$ itself is a density function and therefore has to satisfy the following

mathematical conditions: $K(t) \geq 0$ and $\int K(t)\,dt = 1$. The parameter h determines the amount of smoothing of $p(x)$: a small value of this parameter yields a rougher curve, whereas a large value increases the level of smoothing. For a normal density kernel, the one used in the application discussed in this paper, the width h can be selected using the following criterion (called the "normal reference rule") [19]:

$$h_{REF} \approx 1.06\,\sigma l^{-1/5} \tag{19}$$

where a suitable estimate for σ is the standard deviation. This treatment can be easily generalised to multivariate probability distributions giving, for the case of a Guassian Kernel, the following expression

$$p(\mathrm{x}) = \frac{1}{l\,(2\pi)^{n/2}\prod_{k=1}^{n} h_k} \sum_{i=1}^{l} exp\left\{-\frac{1}{2}\sum_{j=1}^{n}\left(\frac{x_j - X_{ij}}{h_j}\right)^2\right\} \tag{20}$$

The same examples used to train the SVM classifiers can also constitute the elements of the probability density estimation with the Parzen window. Two different probability distributions can be calculated, one for the H mode $p_H(x)$ and one for the L mode $p_L(x)$. Then any new example Xn can be classified by calculating which of the two probabilities, $p_H(Xn)$ or $p_L(Xn)$, is higher.

The two approaches just described, SVM and probability density estimators, provide very good results in terms of success rate but there are margins for improvement. The main idea behind "hybrid methods" consists of combining different classifiers using Bayes decision theory. Given the task of determining to which of M classes, $\omega_1, \omega_2, \ldots, \omega_M$, a new feature vector $\mathbf{x}$ belongs, the final decision can be made using Bayes rule

$$P(\omega_k \mid \mathrm{x}) = \frac{p(\mathrm{x} \mid \omega_k)P(\omega_k)}{p(\mathrm{x})} \tag{21}$$

In practice, the *posterior probability* that the unknown pattern belongs to the respective class w_k, is expressed by the Bayes formula in terms of the likelihood $p(\mathbf{x}|\omega_k)$ and the a priori probability $P(\omega_k)$. The hybrid approach applied to the discrimination of the confinement regime consists of considering first the distance from the separation hyperplane, derived by the SVM, as the a priori probability $P(\omega_k)$ after proper normalization. Secondly, the probability density estimator derived with the Parzen window is interpreted as the likelihood $p(\mathbf{x}|\omega_k)$. Again for each new example to classify, the probability of it being a case of H or L mode of confinement is calculated, with two specific hybrid classifiers as just described, and then the class with the higher probability is chosen. The detailed of the methods and the relative calculations can be found in [3]. Here we simply report the most important results in table II. The success rates for SVM with both linear and nonlinear (Radial Basis Function RBF) kernels are compared with the density estimator using the Parzen window and a hybrid classifier (density estimator plus SVM with RBF kernel). The performance of

the hybrid classifier is clearly the best for both the L to H and the H to L transition. The extremely high success rate motivated directly the systematic use of the approach on wide database and the deployment in concrete real time applications.

3. DISRUPTION PREDICTION

Disruptions are sudden losses of global plasma stability, which lead to abrupt confinement degradation and the termination of discharges in Tokamak devices. In addition to slowing down or even compromising the research programme, they can cause damage to the plasma facing components and even constitute a hazard for the structural integrity of the machines [20]. Various instabilities can trigger disruptions and force the plasma out of its safe operational space even on time scales of the order of milliseconds. Up to now, control of these instabilities has proven to be elusive and disruptions constitute an unavoidable aspect of Tokamak operation particularly in high performance configurations.

The detailed understanding of the plasma evolution, from the onset of the dangerous instabilities to the final triggering of disruptions, is an extremely difficult task. The physics of these instabilities is very often highly complex and nonlinear and the relevant information for prediction and control must be extracted from an enormous amount of signals, routinely acquired in a Tokamak. Since no theoretical model is available to detect the incoming of a dangerous situation, in the last decade, various machine learning techniques, mainly Neural Networks and Support Vector Machines, have been tried for disruption prediction. These computational tools are trained using known examples and they can therefore be tuned to learn from the data and recognise the specific behaviour they were designed to identify. The data driven models of disruptions obtained so far have been more useful for the physical understanding but have rarely been tested in real-time situations, where the need of predicting disruptions extends to the whole evolution of the pulse.

For the analysis reported in this section, the complete evolution of every shot has been followed to detect the approach of a disruption. In the set of discharges originally selected, all the pulses with the available diagnostic information have been considered. The training and test sets, summarised in table III, have been selected completely randomly to avoid any bias. In detail, 80% of the disruptive shots (263 discharges) and 80% of the non disruptive shots (175 discharges) of the training database have been chosen randomly for the training process.

The most important signals for disruption prediction have been identified using a nonlinear correlation technique based on the CART method. The final thirteen signals retained are reported in table IV. In any case, the vast majority of these signals had also been employed in previous investigations on the subject and are in general considered a reasonable choice by the experts. Because each measurement has been acquired by a different diagnostic, a simple interpolation has been applied to every signal to standardize the time basis; a sampling rate of 1 kHz has proved to be adequate for the purpose of the analysis.

To represent the relevant characteristics of the 13 signals it is necessary to condense the main

features of a shot in a compact way. This feature extraction procedure is based on the results of a previous investigation [21]. There each signal has been divided in temporal segments of 30 ms, a time interval that proved to be long enough to show plasma tendencies. These 13 temporal segments are concatenated in a single "feature vector" per pulse after suitable normalization. In the present case, a visual inspection indicates that the high frequency components in the signals become more important close to the disruptions. Consequently, the FFT (Fast Fourier Transform) has been applied to each temporal segment and only the standard deviation of the positive frequency spectrum has been retained."

After the selection of the features vectors as just described, the training of the classifiers has been performed by providing the learning systems with the two classes of inputs: the aforementioned features for time slices belonging to disruptive and non disruptive discharges.

One of the main innovative aspects of the approach described in this section has been the choice of training a series of SVM predictors optimised for various intervals before the disruptions. These predictors are then deployed in parallel, each one analysing a different time interval of the signals being measured during the evolution of the discharge. The main idea is illustrated graphically in figure 5. Each predictor has been optimized for a different 30 ms slice of the discharge and they are then used to analyse the corresponding time interval of the shot.

Originally, to cover the whole possible window of interest, 7 intervals of 30 ms each have been considered ([-60,-30], [-90,-60], [-120,-90], [-150,-120], [-180,-150], [-210, -180], [-240,-210] where the various numbers indicate the ms before the occurrence of the disruption). In the end the sequence of the first three classifiers has proven to provide the best results.

In any case, the number of predictions provided by the sequence of classifiers is equal to the number of classifiers. Moreover, being the SVMs independent, each one provides a different prediction about the incoming of a disruption. Therefore, a decision function is necessary to determine automatically whether an alarm has to be triggered or not. The implementation of this function with another SVM system, using as inputs the outputs of the n SVM classifiers analysing the plasma signals, is the second main innovative aspect of the described technique.

The details of the procedure used to develop this additional SVM implementing the decision function are reported in [22]. The overall results of this predictor based on a two layers of SVM systems are quite positive. They are reported for all the various sequences of the seven original predictors in table V. It can be seen that, as mentioned before, the sequence of three SVM predictors provides the best results, since it probably strikes the best balance between simplicity and completeness of information. The global success rate of about 93% and the level of less than 1% of missed alarms are very encouraging. It is worth mentioning that the global predictor has been optimised with the aim of minimising the number of missed alarms, implicitly considering machine protection the top priority. In case of experimental programmes with other objectives and reduced risks of damage, of course a different trade off could be found to maximise the scientific exploitation of the device.

The success rate and the false alarms obtained for a series of JET experimental campaigns are shown in figure 6. The interval covers the period of JET operation under EFDA from the first campaign in the year 2000 up to C19, which took place in 2005. The predictor has been tested with example up to campaign C7 in 2002 and it has then been applied to the following campaigns without any further adjustment. The decline in performance with time is very slow. The relatively unusual low performance in C11 can be explained in terms of the characteristics of this campaign. C11 was the 2003 Trace Tritium Experiments, in which particular attention was devoted to avoid disruptions. Since the predictor has been optimised to minimise missed alarms at the price of more false alarms, in this campaign the extremely low number of disruptions decreases the statistical performance of the method. The increase in the false alarms after C14 can easily be explained by various modifications of JET implemented in the shutdown just after that campaign, which have implied significant changes in the signals acquired and in the type of configurations run on the machine. The ones affecting the predictor most are: a) the increase in the elongation and triangularity allowed by the Load Bearing Septum Replacement Plate b) the most frequent use of Error Field Correction Coils affecting the Mode Lock signal 3) the installation of a new bolometer system that provides different signals the predictor was originally trained with.

These results are extremely relevant because, contrary to most previous works, in the present case the complete evolution of the considered discharges is followed from the beginning to the end, without any selection of the time slices. Moreover the predictor provides robust results in terms of success rate even for shots performed years after the ones used for the training. The applied database is also the biggest used so far at JET for studying real-time disruption prediction using learning systems since it includes more than 2100 discharges.

4. IMAGE PROCESSING

In the last years, the continuous progress in camera technologies has further motivated the use of these instruments for plasma diagnostics. Video movies indeed provide a lot of information in a form which is particularly intuitive for scientists to interpret, even if extracting quantitative information from the images can be a complex task. Cameras have therefore become much more common tools to monitor the radiation emitted from the plasma and the first wall, both in the visible and in the infrared range of frequencies. On the other hand, the use of images for feedback control is still in its infancy in the fusion community. In JET a new technology has been tested with the dual purpose of processing heavy images in short time and to test a potentially radiation hard technology. The implemented solution is based on Cellular Nonlinear Networks (CNNs), which in our application are two dimensional arrays of dynamical systems called cells (see figure 7) [4]. Various linear and nonlinear operations can be performed on the cells, taking into account also the values of the neighbours, within an interval which can be defined by the user. These operations, called templates, are now provided in suitable libraries and allow performing a wide set of basic calculations on the cells. One of the main advantages of this architecture resides in its parallel

nature, which can be very useful in tasks like image processing for real time, which can pose severe requirements on the computational power. The flexibility of the CNN approach in any case has promoted a wide series of applications, raging from the solution of nonlinear differential equations to robotics and the simulation of biological systems.

In the application tested at JET and whose results are reported in the following, the implementation of the CNN architecture is the chip platform ACE16K [23]. This chip consists of two layers of CMOS components: the first one is a traditional CMOS sensor like those used in commercial digital cameras. The second layer consists of a series of capacitors and resistors implementing the CNN architecture, to perform the desired operations on the individual pixels. A picture of the chip is reported in figure 8. The chip so far has been utilised as a parallel processor to perform several operations on the images provided by JET wide angle infrared camera. One of the most interesting applications consists of the real time detection of the hot spots, which can be induced on JET plasma facing components by concentrated losses due to various operational reasons. The main rationale behind the application is the need to detect when the temperature of parts of the wall exceeds machine protection limits and therefore remedial action has to be undertaken. A series of algorithms have been developed to automatically analyse the IR frames. They typically consist of a first thresholding step, to extract only the higher emitting points, followed by an analysis meant to determine the actual danger of the high temperature regions. Some of the most successful solutions for this real time image processing are described in detail in [24]. In figure 9 the hot spots detected by the CNN are compared with an IR image of JET wide angle camera, where the hottest parts are identified by the brightest emission. The good accuracy of the CNN detection is apparent in this picture and has been verified statistically. The computational time required for a full analysis of the entire frame is of less than 60 ms, more than adequate for machine protection given the relative long time scales of thermal phenomena in a large Tokamak. It is worth mentioning that the CNN technology is not the most widely used and it is not particularly supported by the market. The main objective of the study was more the proof of principle of the algorithms for the real time detection of the hot spots than the qualification of the technology. In the future, the algorithms will be transferred to other alternatives like FPGAs, to insure that solid market technologies are available to implement the detection methods.

5. CONTROL FOR PHYSICS UNDERSTANDING

5.1. REAL TIME TRACKING OF TAE MODES

Up to now the main feedback control strategies applied to the Tokamak configuration have been aimed mainly at operational and protection objectives. Goals like controlling the shape of the plasma boundary or sweeping the position of the strike points to reduce power loads are essential aspects of the operation of a reactor relevant device but are not explicitly conceived to improve the understanding of the physics involved. On JET in the last years, significant efforts have been devoted to the application of control strategies also to improve the understanding of physical phenomena. One of the principal activities in this direction has benefited from the installation of two new sets of Toroidal Alfven

Eigenmode antennas, each one comprising of four loops. These sets have been explicitly designed to excite superalfvenic modes with a toroidal mode number up to about 10, in order to cover the interval of interest for ITER [5]. These antennas inject suitable frequencies into the plasma, which are capable of exciting instabilities of the Alfven type. Once these instabilities start growing by absorbing energy from the waves injected by the antennas, they can be detected using traditional pick-up coils, as shown in a simplified pictorial form in figure 10.

From the point of view of real time control, one of the most interesting experiments consists of the tracking of the frequency of these superalfvenic modes, by sweeping the frequency of the exciting antenna around the resonance frequency. This allows not only following the drift of the mode frequency but more generally to measure the dynamic response of the absorption peak. From the width of the absorption peak, the damping rate of the modes can be determined, which is an essential parameters to assess the behaviour of these modes and their potential negative impact on the confinement of the alpha particles in ITER [6]. An example of the real time tracking of one of these Toroidal Alfven Eigenmodes is shown in figure 11. As can be seen by this example, the main original aspect of this real time control scheme is the objective, which clearly consists of deriving direct information about the physics of a class of instabilities, in particular their damping rate. This is a completely different task than the control of global plasma parameters for machine protection or operational purposes.

5.2. SIMULTANEOUS CONTROL OF THE CURRENT AND KINETIC PROFILES

Another ambitious real time control scheme, meant not only to obtain certain plasma conditions but also to improve the physics understanding, is the simultaneous control of the current and kinetic profiles. Simultaneous control of the plasma shape, the magnetic and kinetic plasma profiles (such as the safety factor, q(x), and gyro-normalized temperature gradient, ρ_{Te}*(x), respectively) and the boundary flux is being investigated on JET, and has potential impact on steady state advanced tokamak programme in ITER. The control of radially distributed parameters was achieved for the first time on JET in 2004 [25-26]. The controller was based on the static plasma response only. The approach newly implemented on JET aims to use a dynamical plasma model, all the available heating and current drive (H&CD) systems, and the poloidal field (PF) systems in an optimal way to achieve a set of requested magnetic and kinetic profiles.

The structure of the model stems from a set of transport equations,

$$\mu_0 \frac{\partial j}{\partial t} = -\nabla \times \nabla \times E, \qquad \frac{\partial n}{\partial t} = -\nabla . \Gamma + S_n, \qquad \frac{3}{2}\frac{\partial (nT)}{\partial t} = -\nabla . Q + S_T \qquad (22)$$

in which couplings are retained for the sake of generality. S_n and S_T are the source terms for the electron density and temperature respectively. The system of equations (22) is linearised around an equilibrium reference state so that it can ultimately be cast in the generic form of a state space model. For the purpose of this linearisation, the natural state variables are the variations of the internal poloidal magnetic flux, Ψ, and of the temperature, T, and the state space model reads:

$$\partial \Psi / \partial t = A_{11} \Psi(t) + A_{12} T(t) + B_{11} P(t) + B_{12} n(t) + U.V_{ext}(t)$$
$$\varepsilon \partial T / \partial t = A_{21} \Psi(t) + A_{22} T(t) + B_{21} P(t) + B_{22} n(t) \quad (23)$$

with inputs $P = [P_{LH}, P_{NBI}, P_{ICRH}]$, the heating and current drive input powers, and V_{ext}, the surface loop voltage. The distributed variables $\Psi(x)$ and $T(x)$, where x is a radial coordinate, are projected onto a finite set of trial functions using a Galerkin scheme so that the original partial differential system of equations reduces to an ordinary linear differential system, where U is known and $A_{i,j}$, $B_{i,j}$ are matrices of appropriate dimensions, which are to be identified from experimental data. The small (constant) parameter, ε, represents the ratio between the energy confinement time and the characteristic resistive diffusion time ($\varepsilon << 1$).

To take advantage of the small parameter ($\varepsilon \approx 0.05$ in JET), the control technique is based on the theory of singularly perturbed systems and multiple-time-scale expansions. This further development consists of trying to optimize two models of reduced orders, a slow model,

$$\partial \Psi / \partial t = A_s \Psi + B_s u_s \quad \text{together with} \quad T_s = C_s \Psi + D_s u_s \quad (24)$$

and a fast model

$$(\tau = t/\varepsilon), \quad \partial T_f / \partial \tau = A_f T_f + B_f u_f \quad (25)$$

where $T = T_s + T_f$, and where u_s and u_f are the slow and fast components, respectively, of a vector, $u = u_s + u_f$, containing all the inputs (P, n and V_{ext}).

Having identified a set of relevant state variables, it can prove advantageous to apply the control to some output parameters which are more directly linked with MHD stability or internal transport barrier physics. The inverse of safety factor, i (x), and gyro-normalized temperature gradient, $\rho_{Te}^*(x)$ [27], have been chosen and are thus introduced into the state-space model. As for $\Psi(x)$ and $T(x)$, a Galerkin approximation is used and in the following, the notations Ψ, T, μ and ρ will refer to the coefficients of the $\Psi(x)$, $T(x)$, $\iota(x)$ and $\rho_{Te}^*(x)$ expansions, respectively. Noticing that $\iota(x) \propto \nabla\Psi(x)$ and $\rho_{Te}^*(x) \propto \nabla\Psi\, Te(x)/\sqrt{Te(x)}$_, linearising these expressions, differentiating the basis functions and assuming that the time variations of factors such as the toroidal magnetic field and toroidal magnetic flux are not essential and do not depend intrinsically on the power inputs, it appears natural to seek a model with direct matrix relations between the Galerkin coefficients of Ψ and μ, on one hand, and between T and ρ on the other hand. Within the two-time-scale approximation, this yields:

$$\mu = C_{\mu,\psi}.\Psi \quad \text{and} \quad \rho_s = C_{\rho,\psi}\Psi + D_{\rho,\psi} u_s \quad (\text{or} \quad \rho_s = C_{\rho,\mu}\, \mu + D_{\rho,\mu}\, u_s) \quad (26)$$

$$\rho_f = C_{\rho,T}.T_f \quad (27)$$

which complete the system of equations 24-25. $C_{i,j}$ and $D_{i,j}$ are the transfer matrixes of the quantities specified by the indices i and j. The identified two-time-scale model is then used to construct and design a controller, which can respond faster to rapid plasma events, while converging slowly towards the requested high performance plasma state (on the resistive time scale) [28].

Open loop modulations of the actuators have been performed around a reference state in order to identify the plasma model. A highly triangular ($\delta = 0.45$) configuration has been chosen to perform both open and closed loop experiments with a toroidal magnetic field of 3T, a plasma current of 1.5MA and an average density of about 3.5×10^{19} m^{-3}.

Control of q profile has been performed over a period lasting more than 7s using the 3 H&CD systems while keeping the loop voltage at a constant value (see Figs. 12 & 13). These preliminary forms of control of the q profile are pioneering results, achieved for the first time on JET. The systematic application of this control scheme has been hampered mainly by two problems. The most severe has certainly been the lack of margins in the actuators. During the experiments the additional heating systems have been marginally capable of producing the power with the required reliability. This aspect has been strongly improved in the last campaigns and should become less of an issue with the routine operation of the present upgrade of the ICRH antennas and the neutral beams. Sometimes in the past also some diagnostics, particularly the polarimeter, have not been able to produce data of a completely satisfactory quality. This difficulty is being addressed using more sophisticated data analysis tool of the type described in the rest of this section.

6. ADVANCED SIGNAL PROCESSING: ADAPTIVE FILTERING

In the case of feedback schemes for the understanding of the physics, like the two described in the previous section, the requirements in terms of measurements can be very stringent. In traditional real time control for operations, very often a limited accuracy in the results can be tolerated provided the practical goals aimed at are properly achieved. In the case of physical studies, the problems to be investigated are typically much more sensitive to the details and therefore the quality of the measurements needs to be of a very high level. Very often the diagnostics have to be pushed to the limits and even transient spurious effects can jeopardize the objectives of the control strategies. The previous example of the current profile control is a case in point, since the real time measurements of the internal poloidal field are certainly one of the most challenging tasks for real time diagnostics on a Tokamak. One experimental technique to obtain information about the current profile is based on the Motional Stark Effect (MSE). The diagnostic measures the radiation emitted by the particles of a neutral beam, a heating beam in the case of JET, which is injected into the plasma. The line emission of the radiation is split in wavelength, the motional Stark effect [29], due to the presence of a quite strong Lorentzian electric field (of the order of a few MV/cm to be compared with a plasma radial electric field of the order of 100kV/cm). Indeed, assuming the Lorentzian electric field experienced by the beam particles ($\mathbf{E} = \mathbf{v_b} \times \mathbf{B}$, where $\mathbf{v_b}$ is the velocity of the particles and $\mathbf{B}$ the local magnetic field) is larger than the electrostatic field of the plasma, it is possible to derive information about the

local poloidal component of the magnetic field since the velocity of the beam particles is known (see figure 14).

In the implementation at JET, the red shifted π^+ component of the D_α emission, with polarization angle γ parallel to **E**, is analysed with polarimetric techniques. For each line of sight, a series of interference filters and two photoelastic modulators followed by an avalanche photodiode are used. The detection scheme with the main frequencies of the modulation is shown in figure 15.

For the purposes of this paper, the only relevant aspect of the detection is the fact that the angle γ to be measured is in fact linked to the various modulated components of the current at the output of the photodiode by the relation:

$$\tan(2\gamma(t)) = \frac{C_{21} A_{DC}(t) + C_{22} A_{23}(t) + C_{23} A_{46}(t) + C_{24} A_{40}(t)}{C_{11} A_{DC}(t) + C_{12} A_{23}(t) + C_{13} A_{46}(t) + C_{14} A_{40}(t)} \tag{28}$$

where the Aij are the amplitudes of the various modulated frequencies and the Cij are simple constants to be determined during the calibration of the diagnostic.

The described configuration of the diagnostic works very well in the Ohmic or L mode configurations and in general when the Edge Localised Modes (ELMs) are small. On the other hand, it can strongly be affected by the intense radiation emission due to large ELMs. An example of the problem is reported in figure 16, where it can be seen how an ELM can induce a spurious signal much higher than the real one, seriously compromising the output of the detectors, particularly in the case of real time applications, when ad hoc post processing is not an option. In order to overcome this issue, a form of adaptive filtering is necessary since the level of spurious radiation changes of about one order of magnitude in different periods of the same discharge.

To alleviate this problem a filter of the Kalman type [30] has been designed, optimised and implemented on JET. Indeed a lock-in like model of the measurement is available (equation 28). Therefore the approach of the Kalman filter, which guarantees a minimal error in the least square sense given the noise statistics, is appropriate. The equation for the model estimate of the measurements is of the form:

$$x_k = F x_{k-1} + \mu_k \tag{29}$$

where F is the process matrix and m the process noise. For the measurements the equation is:

$$z_k = H x_k + \varepsilon_k \tag{30}$$

where H is the transfer matrix and e the measurement noise. It is assumed that both μ and ε are uncorrelated zero mean Gaussian distributed white noise. The two equations can be combined to yield the a posteriori estimate $\hat{x}_k$ from the a priori counterpart $\hat{x}_k^-$:

$$\hat{x}_k = \hat{x}_k^- + K_k\left(z_k - H\hat{x}_k^-\right) \tag{31}$$

It can be demonstrated that the optimal gain K_k is:

$$K_k = P_k^- H^T \left(HP_k^- H^T + R\right)^{-1} \tag{32}$$

where

$$P_k^- = FP_{k-1}F^T + Q \tag{33}$$

$$P_k = \left(I - K_k H\right)P_k^- \tag{34}$$

Intuitively, in this JET application, the value of the gain follows a sigmoid function and therefore it is high when the measurements are similar to the model and becomes very low when the measurements are too far away from the model due to the ELM spurious radiation. The global strategy therefore consists of weighting more the measurements when they are not too far away from what is expected. On the contrary, in case of completely different measurements from what expected on the basis of the previous time slice, the model is deemed more realistic and used as the basis for the estimated true value.

The final results are very positive. The Kalman filter has proved to be much more resilient to the ELMs than the previous scheme, founded on the traditional single phase lock-in amplifier method with moving average DC filtering. A representative comparison between the results of the two filters is reported in figure 17, showing clearly the superior quality of the Kalman solution.

CONCLUSIONS AND FURTHER DEVELOPMENTS

On JET several important aspects of information processing for feedback are being addressed. From a technical point of view, various solutions are being tested for the real time identification of the plasma, particularly the confinement regime and the internal topology of the magnetic fields. Machine learning methods for disruption prediction are attracting a lot of attention for the implications on machine protection particularly in the perspective of ITER. Image processing is receiving increased interest, to keep pace with the more systematic use of cameras in Fusion devices.

With regard to the scientific exploitation of JET, new feedback schemes are being pursued to improve the physics understanding of various phenomena from the triggering of ITBs to the impact of TAE modes on the fast particles. They have also motivated the implementation of more sophisticated signal processing tools like the Kalman filter. On the other hand, this is a field in which more could probably be done. Feedback control to study impurity transport or real time control of other instabilities, in addition to the TAEs, are just two aspects, which come immediately to mind.

It is worth mentioning that one of the main future developments, particularly in the perspective of ITER, is the development of more centralized controllers. Operation closer to the limits increases

the links among all the crucial aspects of Tokamak operation. Therefore the typical solution of developing independent controllers, each one in charge of the feedback required by a different subsystem, becomes increasingly dangerous. This approach, shown in the top of figure 18, cannot guarantee to achieve an optimal control and can even run into serious difficulty if contradictory requests are pursued by different subsystems. Therefore the integration of more controllers below the umbrella of a single supervisor becomes progressively more essential. A global view of feedback control will become also more important after the installation on JET of the new ITER-like wall.

From the point of view of control theory, another possible line of research, which could be useful to investigate, is the one of Fuzzy Control. Indeed Tokamak plasmas are very complex and nonlinear systems. Many are the sources of uncertainties, not least the error bars of the measurements. Therefore the potential of Fuzzy logic to handle uncertainties in a robust way could prove to be a very important advantage. In this perspective also the combination of Fuzzy Logic with Neural Networks in hybrid systems could provide interesting results.

ACKNOWLEDGMENTS

This work, supported by the European Communities under the contract of Association between EURATOM and ENEA, CIEMAT, CEA, IPP, CRPP and IST, was carried out under the framework of the European Fusion Development Agreement. The views and opinions expressed herein do not necessarily reflect those of the European Commission.

REFERENCES

[1]. P. Gregory "*Bayesian Logical Data analysis for the Physical Sciences*" Cambridge University Press, 2006, Cambridge, UK.

[2]. Shafranov, V.D. (1966) Plasma equilibrium in a magnetic field, *Reviews of Plasma Physics*, Vol. **2**, New York: Consultants Bureau, p. 103.

[3]. J. Vega et al "*Automated estimation of L/H transition times at JET by combining Bayesian statistics and Support Vector Machines*" submitted to Nuclear Fusion

[4]. L.O. Chua and L. Yang, IEEE Trans. Circuits Syst., I: Fundam. Theory Appl. **35**, 1257, 1988.

[5]. D. Testa et al., The new AlfvÈn Wave Active Excitation System at JET, 23rd Symposium on Fusion Technology (SOFT), Venice (Italy), 20-24 September 2004.

[6]. W.W. Heidbrink, Physics of Plasmas **15**, 055501 (2008)

[7]. Moreau. D., et al., "*Development of Integrated Real-Time Control of Internal Transport Barriers in Advanced Operation Scenarios on JET*", Fusion Energy 2004 (Proc. 20th Int. Conf. Vilamoura, 2004), IAEA-CSP-25/CD, IAEA, Vienna (2005), CD-ROM file EX_P2_5

[8]. A. Zaknich "*Principles of Adaptive Filters & Self-learning Systems*" Springer-Verlag, 2005, London

[9]. Lao, et.al., Nuclear Fusion **30**, 1035 (1990).

[10]. J. Svensson, A. Wemer. "*Current Tomography for Axisymmetric Plasmas*". Plasma Phys. Control. Fusion 50 085002 (2008)

[11]. J. Blum, in IMA Volumes in Mathematics and its applications, Large scale optimization with applications, Part 1: optimization in inverse problems and design, edited by Biegler, Coleman, Conn and Santosa, 1997, Vol 92 pp 17-36
[12]. Wagner, F. et al., Physical Review Letters **49**, 1408 (1982).
[13]. V. Vapnik. "The Nature of Statistical Learning Theory". Second edition. Springer. (1999).
[14]. V. Cherkassky, F. Mulier. "Learning from data". John Wiley & Sons, Inc. (1998).
[15]. Meakins, A.J. (2008) "*A Study of the L-H Transition in Tokamak Fusion Experiments*". PhD Thesis. Imperial College London.
[16]. Breiman L., Friedman J.H., Olshen R.A. and Stone C.J. 1984 *Classification and Regression Trees* (Belmont, CA:Wadsworth Inc.) (1993, New York: Chapman and Hall)
[17]. G.Vagliasindi, A.Murari, P.Arena, L.Fortuna and JET-EFDA Contributors. "*Automatic Derivation of an Interpretable Fuzzy Logic Classifier from Classification and Regression Trees with application to Confinement Regime identification in Nuclear Fusion*". In submission to IEEE Transactions on Fuzzy System.
[18]. R.O. Duda, P. E. Hart, D.G. Stork. "Pattern classification". Second edition. Wiley-Interscience. (2001).
[19]. W.L. Martinez, A.R. Martinez. "Computational Statistics Handbook with MATLAB". Chapman & Hall/CRC. (2002).
[20]. F.C. Schuller 1995. "*Disruptions in tokamaks*". Plasma Phys. Control. Fusion. 37 A135-62.
[21]. G.A. Rattá et al Rev. Scient. Instruments **79**, 10F328 (2008)
[22]. G.A. Rattá et al, "*An Advanced Disruption Predictor for JET tested in a simulated Real Time Environment*" submitted to Nuclear Fusion
[23]. A. Rodríguez-V·zquez, G. Linan-Cembrano, L. Carranza, E. Roca-Moreno, R. Carmona-Galan, F. Jimenez-Garrido, R. Dominguez-Castro, and S. Espejo Meana, IEEE Trans. Circuits Syst., I: Fundamental Theory Applications **51**, 851 (2004).
[24]. P.Arena et al Rev. Scient. Instruments **76**, 113503 (2005)
[25]. Laborde, L., et al., "*A Model-Based Technique for Integrated Real-Time Profile Control in the JET Tokamak*", Plasma Phys. Contr. Fus. **47** (2005) 155.
[26]. Mazon, D., et al., "*Active Control of the Current Density Profile in JET*", Plasma Phys. Contr. Fus. **45** (2003) L47.
[27]. Tresset, G., et al., "*A Dimensionless Criterion for Characterising Internal Transport Barriers in JET*", Nuclear Fusion **42** (2002) 520.
[28]. Moreau. D, D. Mazon et al., '*A multiple time scale dynamical approach for magnetic and kinetic profile control in advanced tokamak scenarios*', Nuclear Fusion Vol **48** (2008) 106001 (38pp).
[29]. F.M. Levinton, R.J. Fonck, G.M. Gammel, R. Kaita, H.W. Kugel, E.T. Powell, and D.W. Roberts, Phys. Rev. Lett. **63**, 2060 (1989)
[30]. R. Coelho and D. Alves, IEEE Trans. Plasma Science **37**, 164, (2009)

Transition	Signal	Signal description
L/H	Bndiam	Beta normalised with respect to the diamagnetic energ
	Ptot	Total heating power
	Wmhd	Magneto-hydrodynamic energy
	RXPL	R coordinate lower X point
	ZXPL	Z coordinate lower X point
	Bt80	Axial toroidal Magnetic Field at a psi = 0.8 surface
H/L	Bndiam	Beta normalised with respect to the diamagnetic energy
	Bt	Toroidal magnetic field
	FDWDT	Time derivative of diamagnetic energy
	Q95	Safety factor
	RXPL	R coordinate lower X point
	ZXPL	Z coordinate lower X point

Table I : The most important signals for the study of the L to H and H to L transitions as determined with the CART algorithm.

	L/H transitions	H/L transitions
SL	96.61%	89.38%
SR	99.11%	94.44%
(245)	$\sigma = 10$	$\sigma = 39$
PW	98.61%	95.88%
(60)	$0.5h_{j,REF} \leq H \leq 0.71h_{j,REF}$	$h = 0.95h_{REF}$
	$\sigma = 10$	$\sigma = 39$
BSR	99.17%	96.25%
	$h0.5h_{REF}$	$h0.53h_{REF}$
	$k = 27$	$k = 2$

Table II : Success rates achieved for the test set and different classifiers: SL (SVM, linear kernel), SR (245 classifiers based on SVM and RBF kernels), PW (60 models based on Parzen window estimators) and BSR (Bayes/SVM (RBF kernel) combination).

Databases	Number of discharges
Disruptive train	263
Non disruptive train	219
Disruptive test	66
Non disruptive test	44
Total disruptive	329
Total non disruptives	219
Total discharges	548

Table III: The discharges used to train and test the SVM disruption predictor.

	Signal name	Units
1.	The plasma current.	A
2.	The poloidal beta.	
3.	The poloidal beta time derivative.	s^{-1}
4.	The mode lock amplitude.	T
5.	The safety factor at 95% of minor radius.	
6.	The safety factor at 95% minor radius time derivative.	s^{-1}
7.	The total input power.	W
8.	The plasma internal inductance.	
9.	The plasma internal inductance time derivative.	s^{-1}
10.	The plasma vertical position.	m
11.	The plasma density.	m^{-3}
12.	The stored diamagnetic energy time derivative.	W
13.	The net power (total input power *minus* total radiated power).	W

Table IV: The most informative signals for disruption prediction as identified with CART.

	MA	FA	PA	TE	SR	AVG
Sequence 1 (M2, M1)	**0**	**5.4545**	**5.4545**	**10.909**	**89.091**	**128.01**
Sequence 2 (M3, M2, M1)	**0.909**	**4.5455**	**1.8182**	**7.2727**	**92.727**	**146.23**
Sequence 3 (M4, M3,…, M1)	**0**	**4.5455**	**5.4545**	**10**	**90**	**132.23**
Sequence 4 (M5, M4,…, M1)	**0**	**5.4545**	**9.0909**	**14.545**	**85.455**	**128.84**
Sequence 5 (M6, M5,…, M1)	**0**	**4.5455**	**7.2727**	**11.818**	**88.182**	**136.45**
Sequence 6 (M7, M6,…, M1)	**0**	**5.4545**	**5.4545**	**10.909**	**89.091**	**136.23**
Sequence 7 (M8, M7,…, M1)	**0**	**5.4545**	**6.3636**	**11.818**	**88.182**	**121.01**

Table V: The various sequences of SVM classifiers tested and their performance. MA are the missed alarms, FA are the false alarms, PA the premature alarms, TE are the total errors, SR is the global success rate, AVG is the average time before the disruption that the sequence manages to detect the disruption itself. All the various performance estimators are expressed in percentage terms except AVG whose unit is ms. The sequence of classifiers with the best results is shaded.

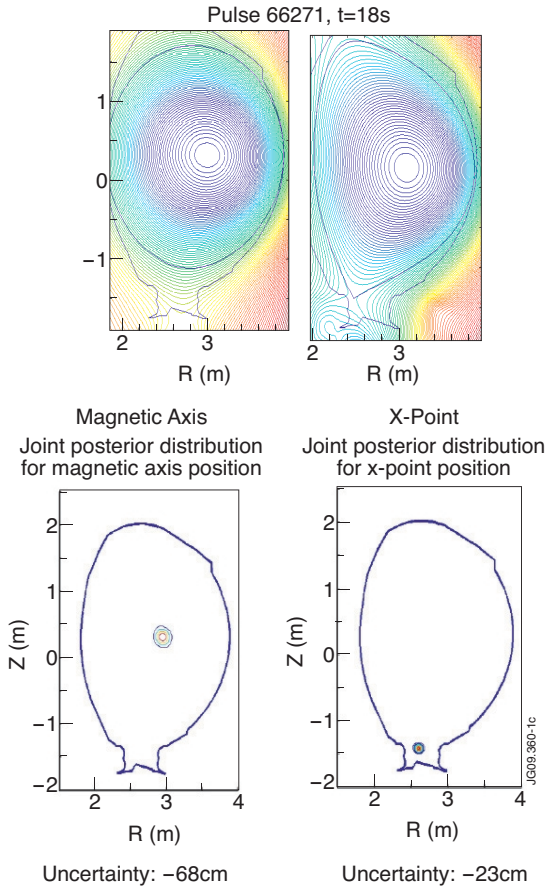

Figure 1: Top: magnetic surfaces reconstructed with the Bayesian method for a limiter configuration (left) and X-point configuration (right). Bottom: uncertainty in two important topological parameters the position of the magnetic axis (left) and X point position (right). JET Pulse No: 66271.

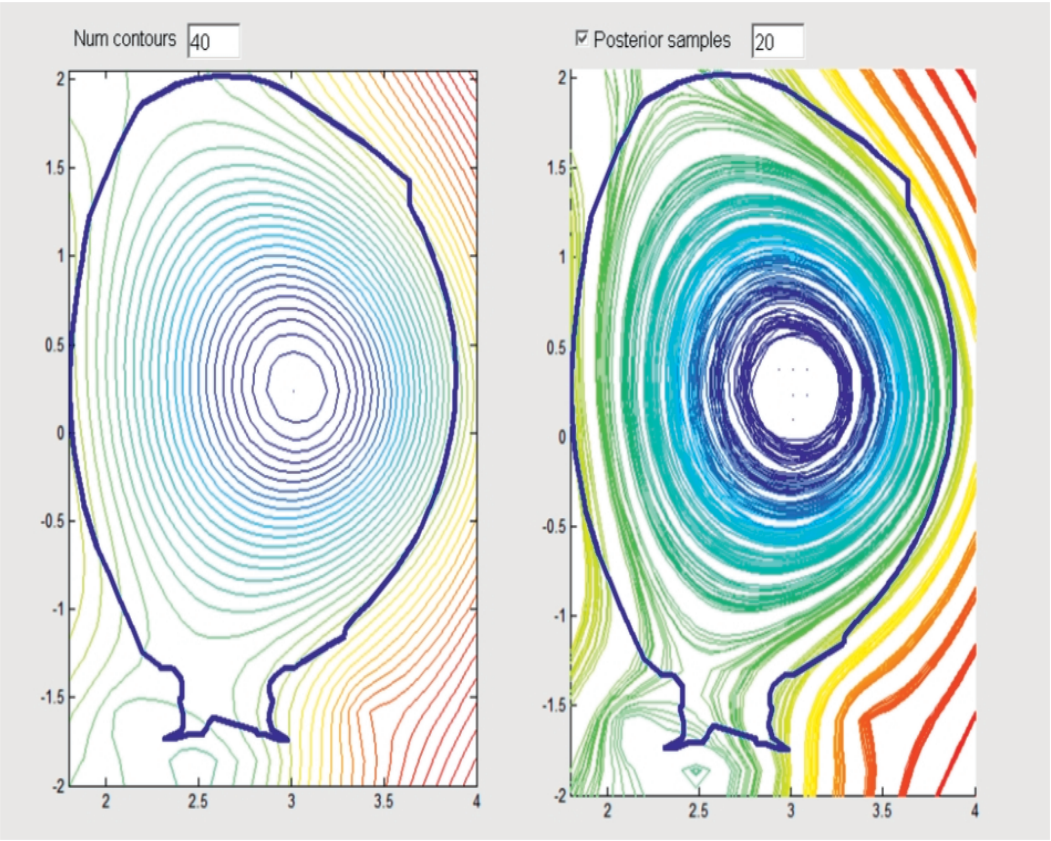

Figure 2: Left: the magnetic topology with the maximum posterior probability Right: the uncertainty intervals on the magnetic surfaces for JET Pulse No: 66271.

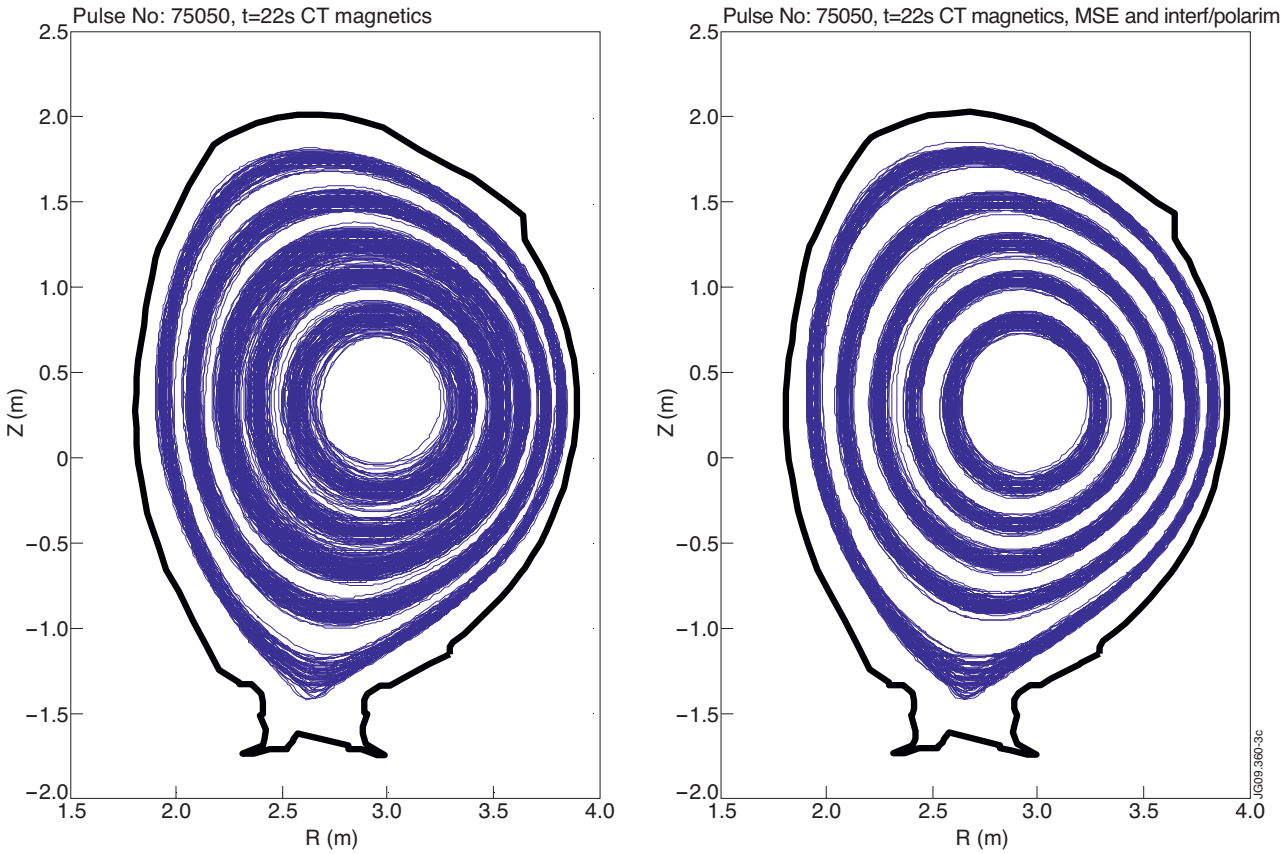

Figure 3: Reduction of the uncertainty intervals on the magnetic topology when additional diagnostic measurements are provided as inputs. Top: uncertainty intervals when only the pick-up coils are used Bottom: uncertainty intervals when also polarimetry and motional Start effect measurements are included in the analysis.

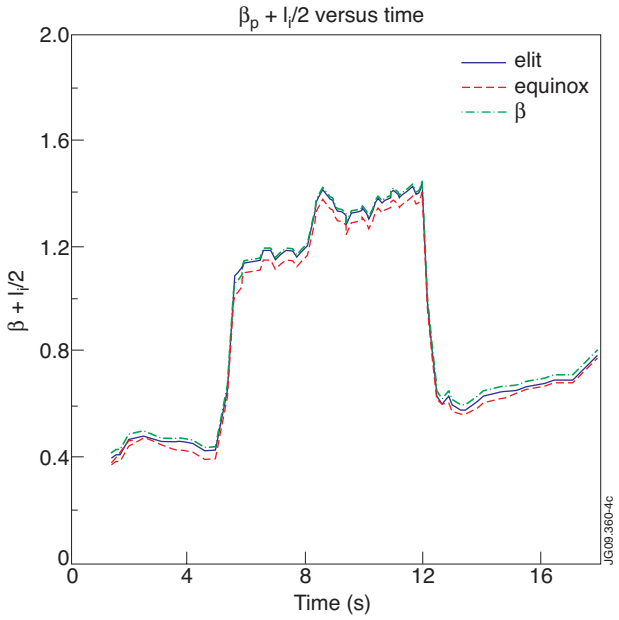

Figure 4: Top: comparison of the time evolution of $\beta_{pol} + l_i/2$ calculated with EQUINOX and two other validated offline JET codes (EFIT and betali). l_i is the plasma internal inductance Bottom: statistical comparison between EQUNOX and XLOC for the distance of the plasma from the internal wall on the equatorial pane (RIG)

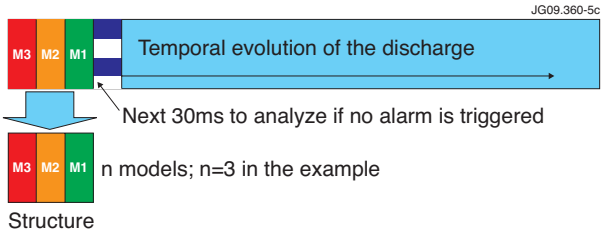

Figure 5 :The sequence of SVM classifiers used to analyse in parallel subsequent time intervals of plasma signals.

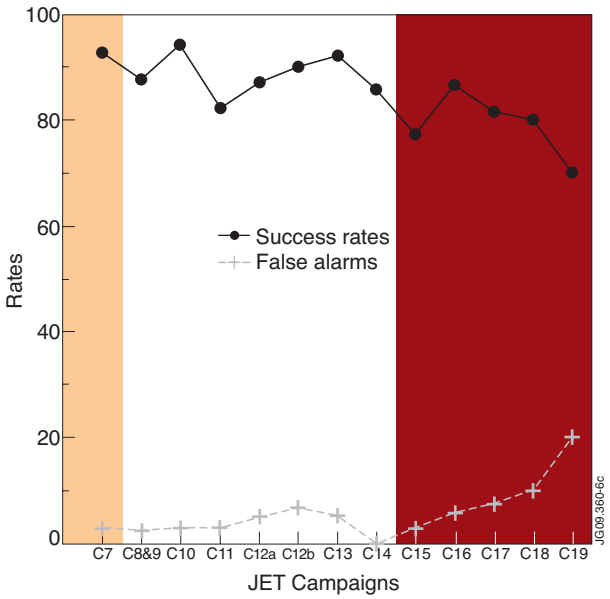

Figure 6: The success rate of the SVM predictor for various campaigns. The pink shaded region on the left indicates the campaigns used for the training. The white intermediate region covers the campaigns not used for the training but without major modifications to the JET machine. Between C14 and C15 significant changes in the device were implemented.

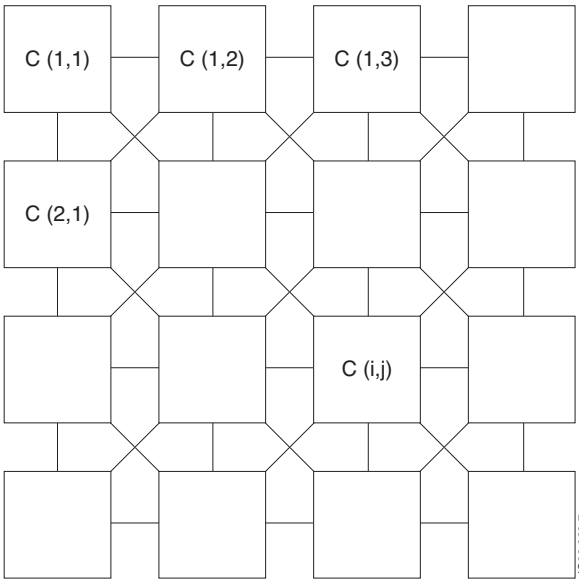

Figure 7: Architecture of a 2D CNN array.

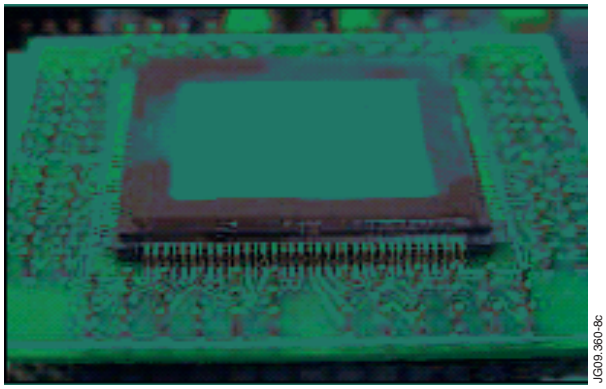

Figure 8: The chip platform ACE16K

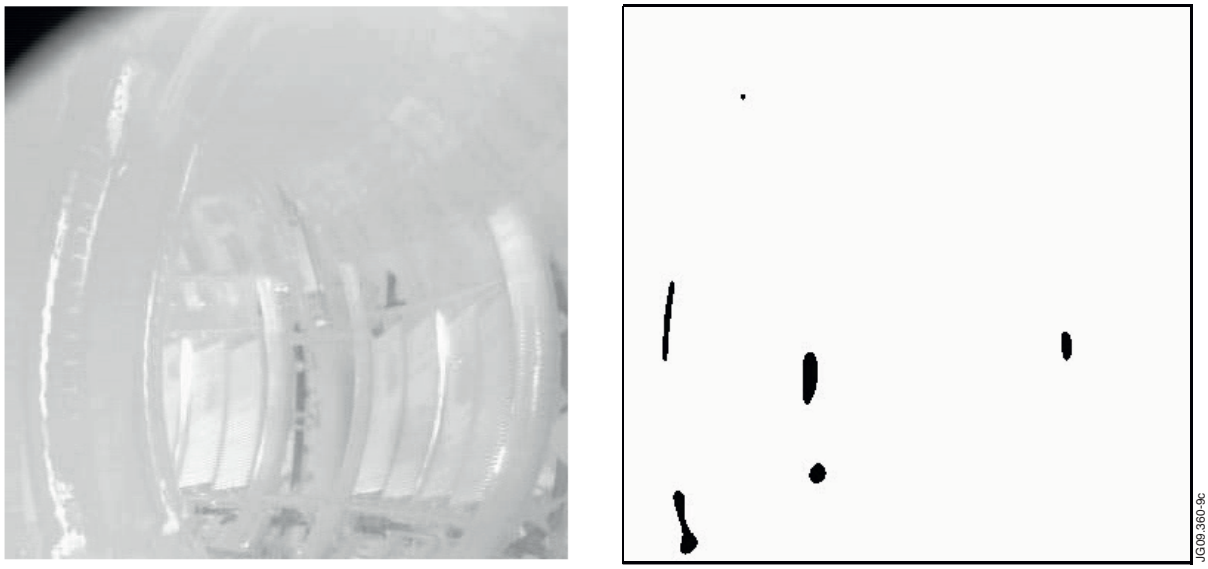

Figure 9: Left: an infrared image taken with JET wide angle camera Right: the hot spots automatically detected by one of the algorithms implemented with the CNN.

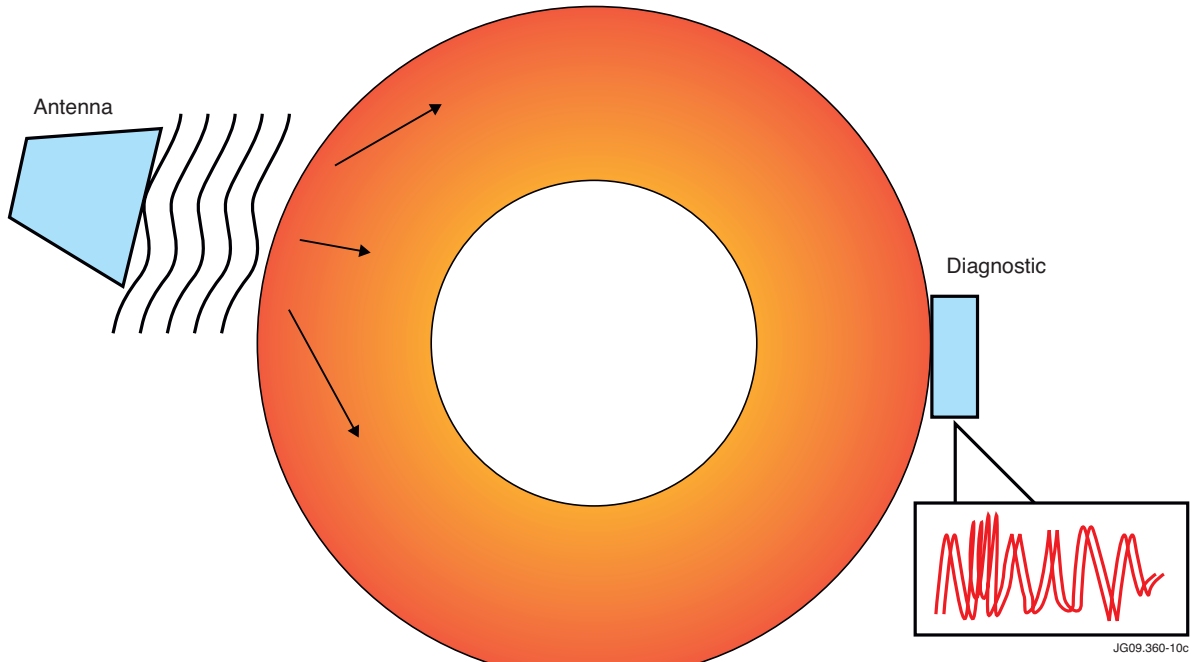

Figure 10: Pictorial view of the excitation of TAE instabilities via injection of waves. The detection is performed with pick-up coils.

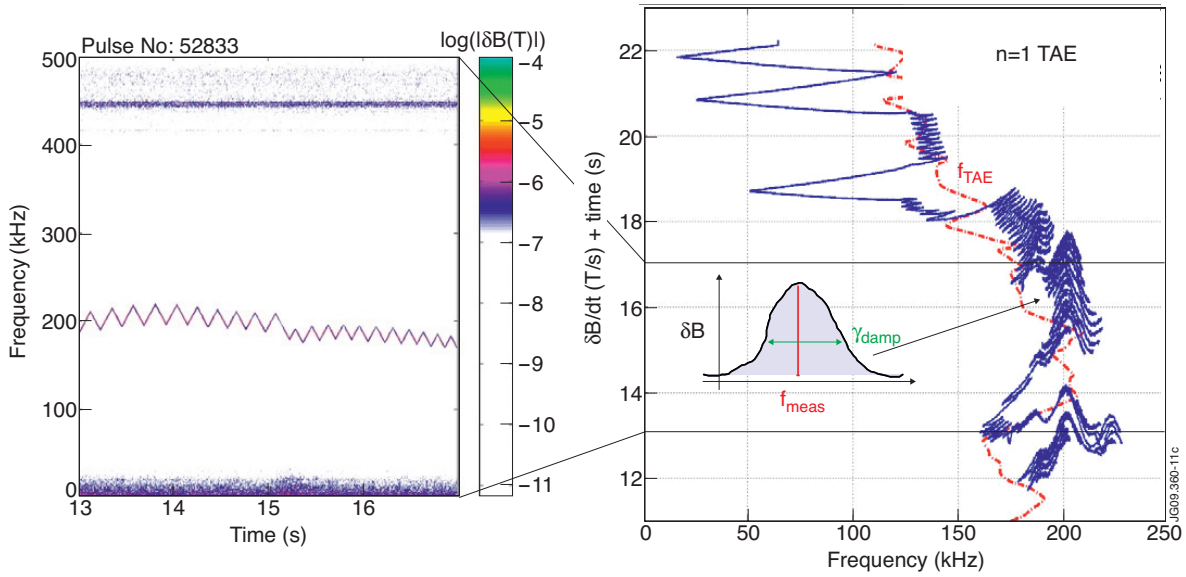

Figure 11: Real time tracking of an Alfven Eigenmode and measurement of the absorption peak. The blue curve on the right plot indicates the shape of the absorption peak around the main mode frequency, from which the damping rate can be derived.

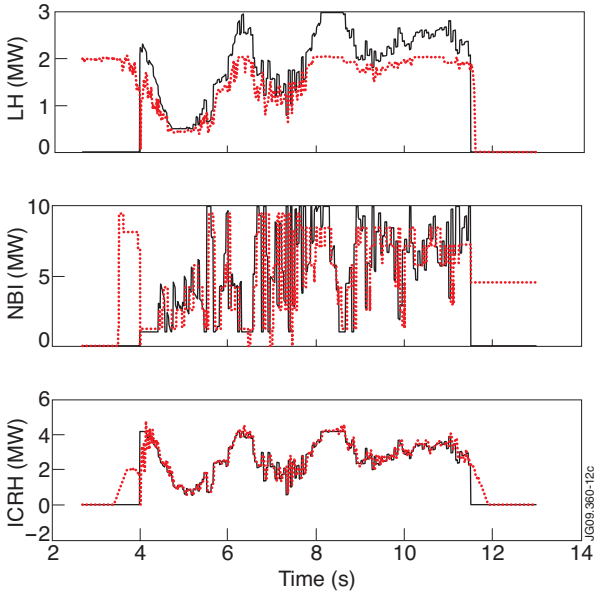

Figure 12: Requested (blue) and delivered (red) powers (LHCD, NBI, ICRH) for the controlled Pulse No: 70395. These plots show how JET heating systems have managed to deliver almost exactly the powers requested of them.

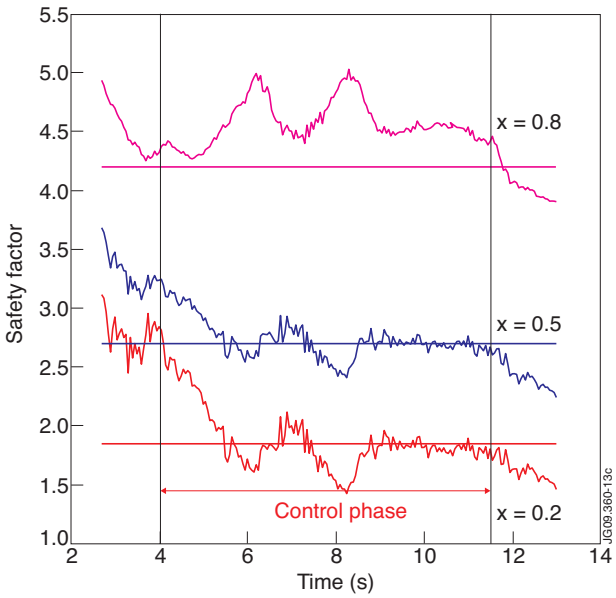

Figure 13: Control of the safety profile at 3 normalised position using the 3 H&CD actuators for Pulse No: 70395. The horizontal lines are the requested values. V_{loop} constant (32 mV/rad).

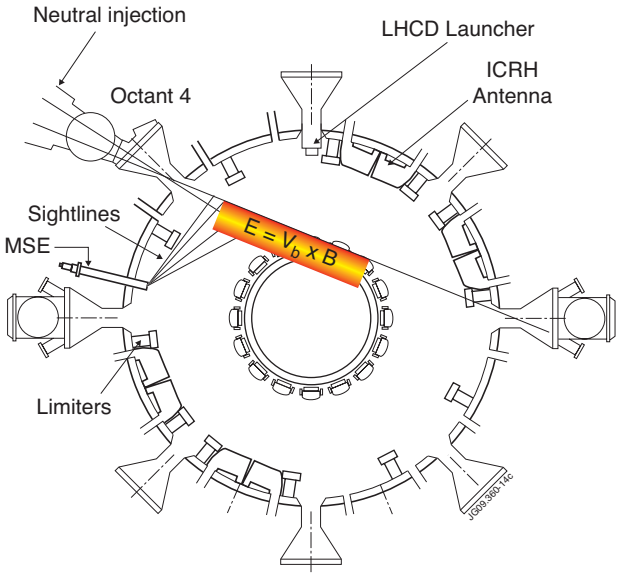

Figure 14 : Layout of the Motional Stark Effect diagnostic at JET.

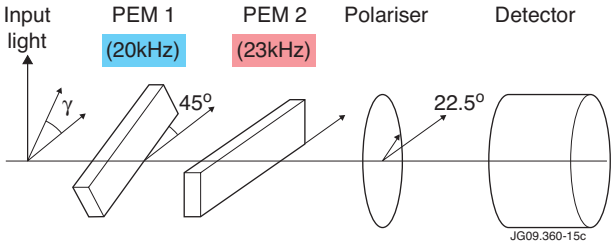

Figure 15: Detection scheme of one channel of JET MSE diagnostic, showing the photoelastic modulators, polariser and detector.

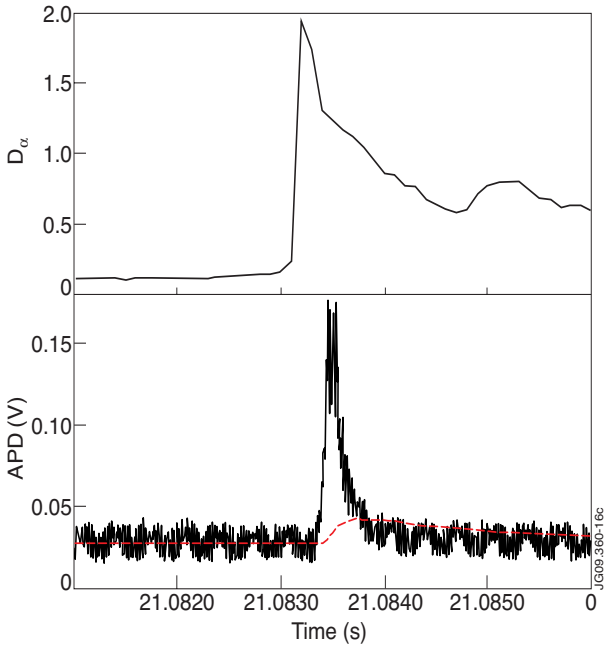

Figure 16: Top: the Da emission during an ELM. Bottom: the spurious radiation on one of the MSE channels. The estimated DC component with ELM correction is indicated by the gray, smoother curve: this is the signal to be used for the calculation of the real Stark effect.

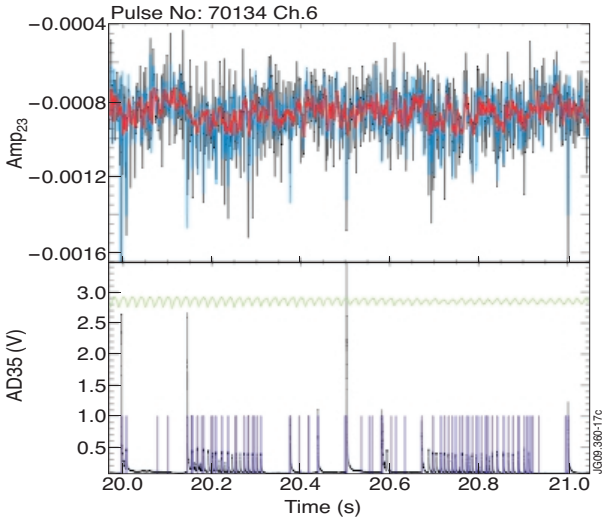

Figure 17: Top: result showing the superior performance of the Kalman filter (red) with respect to the moving average approach (blue). The variations due to the ELMs, identified in the bottom plot by the Da emission, are much lees evident in the signal output of the Kalman filter.

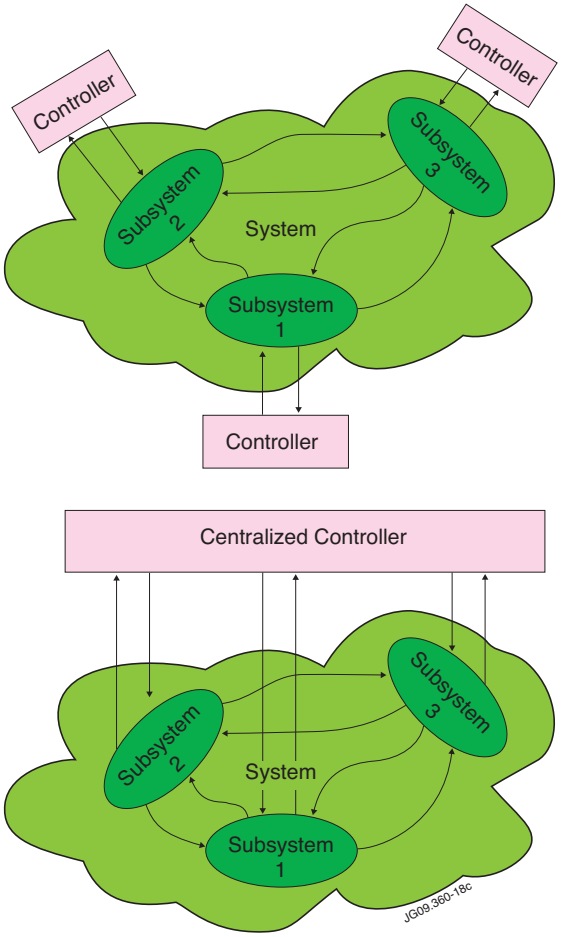

Figure 18: Left: distributed controller Right: centralised controller.